*J. Physiol.* (1986), **373**, *pp.* 63–86
*With 8 text-figures*
*Printed in Great Britain*



# PROJECTION OF PULMONARY RAPIDLY ADAPTING RECEPTORS TO THE MEDULLA OF THE CAT: AN ANTIDROMIC MAPPING STUDY

BY R. O. DAVIES AND L. KUBIN

*From the Department of Animal Biology, School of Veterinary Medicine and Cardiovascular-Pulmonary Division, School of Medicine, University of Pennsylvania, Philadelphia, PA 19104, U.S.A.*

(*Received 4 June 1985*)

SUMMARY

1. The activity of pulmonary rapidly adapting receptor (r.a.r.) neurones was recorded extracellularly in the nodose ganglion of the decerebrate cat. The receptors were identified by their rapid adaptation to ' ramp and hold ' hyperinflations of the lung. The antidromic mapping technique was used to determine the sites of projection and branching patterns within the nucleus of the tractus solitarius (n.t.s.) of eleven r.a.r.s.

2. The medulla was explored with a stimulating electrode to activate the r.a.r.s antidromically. In each penetration, depth–threshold measurements were made for each antidromic response characterized by a distinct latency. Using the anatomical sites of the minimum threshold points, the locations of central branches of individual r.a.r.s were determined. The main axons of all of them coursed within the tractus solitarius (t.s.) at levels from 2 mm rostral to 0·5 mm caudal to the obex. The axonal conduction velocities within the t.s. were 6·2–9·7 m/s, where the peripheral conduction velocities were 11·2–20·4 m/s (28 °C). Different latencies of response evoked in a single penetration were considered to indicate branching. The densest branching was found in the ipsilateral commissural subnucleus of the n.t.s. at levels 0·3–1·3 mm caudal to the obex and, to a lesser degree, in the contralateral commissural subnucleus. All r.a.r.s sent a few branches to the medial n.t.s. rostral to the obex. Four r.a.r.s ramified in the ventrolateral n.t.s. where inspiratory cells are located.

3. Depth–threshold graphs were interpolated by best fitting parabolic equations: $I_{th} = Ad^2 + Bd + C$; where $I_{th}$ is the threshold current, $d$ the corresponding depth of stimulation, and $A$, $B$ and $C$ are coefficients. Coefficient $A$ is a measure of steepness of the parabola. The $A$ coefficients were inversely related to the conduction velocity ($v$) of the stimulated branch. An analysis of the data from the present study ($v$ = 5·0–9·7 m/s) combined with data from the literature ($v$ = 2·2–85 m/s) led to a simple relationship between the $A$ coefficient and the conduction velocity of the stimulated fibre: $A = 6500/v$, where $A$ is expressed in $\mu A/mm^2$ and $v$ is expressed in m/s. Within the range 3–35 m/s, the formula is useful in predicting the effective current spread when the conduction velocity is known, or to estimate the conduction velocity from the shape of a depth–threshold curve.

4. Two slowly adapting pulmonary stretch receptors (p.s.r.s) were studied. No

contralateral projection was detected. The central projection of one p.s.r. was mapped in detail; the densest projection was to the ventrolateral n.t.s., with a few branches to the medial n.t.s.

5. The importance of the medial and commissural subnuclei of the n.t.s. in respiratory reflexes is discussed. Differences in central projection patterns of r.a.r.s and p.s.r.s are analysed.

## INTRODUCTION

Rapidly adapting receptors (r.a.r.s) are airway mechanoreceptors that respond to large, rapid inflations or deflations of the lung with an irregular discharge of action potentials that adapts rapidly when the volume stimulus is maintained. They are also stimulated during hyperpnoea, pneumothorax and anaphylaxis, and by a variety of noxious agents (see Pack, 1981; Sant'Ambrogio, 1982; Widdicombe, 1982 for reviews). Rapidly adapting receptors may be involved in the reflex bronchoconstriction associated with many pathological states, the triggering of spontaneous sighs, the normal control of expiratory duration and airflow, and a facilitation of the phrenic output during normal hyperpnoeic states (see Paintal, 1973; Pack, 1981; Widdicombe, 1982, for reviews). The pathways through which these reflex effects could be produced are unknown. It has been difficult to establish the role of r.a.r.s in the control of ventilation because of the problem of stimulating them directly, without concomitantly activating the other major airway mechanoreceptors, the slowly adapting pulmonary stretch receptors (p.s.r.s).

Previous neuroanatomical investigations in the cat (Kerr, 1962; Cottle, 1964; Kalia & Mesulam, 1980) have shown that vagal afferent fibres, including those from the lungs and airways, terminate principally in the nucleus of the tractus solitarius (n.t.s.). However, such studies did not allow one to distinguish the projection patterns to the various subnuclei of fibres of different sensory modalities. We have begun our study of the r.a.r. reflex pathway by determining the medullary sites of the central projections of individual r.a.r. neurones. For that, we have used the antidromic mapping technique (for review, see Lipski, 1981) to determine the central pathway and regions of termination within the n.t.s. of single, functionally identified r.a.r.s whose activity was recorded in the nodose ganglion. This same method proved successful for the mapping of the brain-stem projection of p.s.r. neurones (Donoghue, Garcia, Jordan & Spyer, 1982). In addition, during the course of this study it became apparent that the properties of the central branches of r.a.r. cells rendered them suitable for analysing the relationship between the excitability of central fibres and their conduction velocities. Thus, a considerable effort was devoted to a quantitative assessment of the threshold–distance relationships for different fibres.

Preliminary reports have been published elsewhere (Kubin & Davies, 1984, 1985).

## METHODS

### *Animal preparation*

The results reported are from experiments on thirteen cats of either sex, weighing 1·8–3·3 kg. The cats were pre-anaesthetized with ketamine (70 mg, I.M.) and given dexamethasone (1 mg, I.M.)

to minimize brain oedema. Following intubation, the animals were anaesthetized with halothane and decerebrated (Kirsten & St. John, 1978). Anaesthesia was then discontinued.

A femoral artery and vein were catheterized for blood pressure recording and drug administration, respectively. The C5 branch of the left phrenic nerve was exposed, cut distally and desheathed for whole-nerve recording. The right cervical vagus nerve and nodose ganglion were exposed by a lateral approach and dissected free from the surrounding connective tissue. The cat was then placed in a stereotaxic frame with the head ventroflexed at 45 deg and a vertebral clamp at T2. After a posterior fossa craniotomy and opening the dura, the cerebellar vermis was reflected rostrad to uncover the obex. The animals were ventilated with a constant-flow pump that could operate either at a pre-set tidal volume and frequency or as a cycle-triggered ventilator, controlled by logic signals derived from the animal's phrenic neurogram (Marino, Davies & Pack, 1981). The cats were paralysed with gallamine triethiodide (initial dose of 10 mg, I.V., supplemented with an I.V. infusion of 5 mg/kg.h). A pneumothorax was made and an expiratory load of 1–2 $cmH_2O$ imposed.

Tracheal $CO_2$ concentrations were continuously monitored using an infra-red analyser (Godart Capnograph) connected to the tracheal cannula; end-expiratory levels were maintained at 3·5–5·0 %. In some experiments oxygen was added to the inspired air. Systemic arterial blood pressure was monitored from the arterial catheter using a pressure transducer (Statham P23Gb). Trachael pressure was measured using a pressure transducer (Statham P23Gb) and air flow with a pneumotachograph (Fleisch 00) and differential pressure transducer (Grass PT5). Tidal volume was determined by electrical integration of the air-flow signals. The rectal temperature was maintained at 37·5–38·5 °C by a servo-controlled heating pad.

*Neural recording and stimulation*

Phrenic nerve activity was recorded with a bipolar, platinum electrode suspended in a pool of mineral oil. The signal was amplified (Grass P511), rectified and processed by a low-pass, third-order Paynter filter with a 100 ms time constant to compute the moving average of the neural activity.

Single-cell activity was recorded extracellularly in the nodose ganglion with aluminium glass micro-electrodes (A–M Systems) filled with 3 M-NaCl. The tips were mechanically broken to give a diameter of 0·8–2·0 $\mu$m (resistance: 1·2–2·5 MΩ). The nodose ganglion was supported on a silver plate, which also served as a reference electrode. The micro-electrodes were advanced by a stepping motor, hydraulic microdrive (Haer). The activity was amplified (Grass P511), displayed on a storage oscilloscope (Tektronix 5113), and fed to a window discriminator. The standard pulses from the discriminator were processed by a microprocessor-based (PCM-12) rate-meter, with a moving time window, to provide a moving average of the cell 's firing rate (window width: 200 ms; advanced in time every 5 ms).

Medullary microstimulation or extracellular multi-unit recordings were made with monopolar, stainless-steel micro-electrodes (Micro Probe, Inc.) having resistances of 0·5–1·5 MΩ. The electrode penetrations were made with a stepping motor, hydraulic microdrive (Haer). The activity was amplified (Grass P511) and displayed on an oscilloscope. Electrical stimulation was done using a Grass S48 stimulator and constant current isolation unit (PSIU6). Monophasic, rectangular current pulses having a duration of 100 $\mu$s and an amplitude not exceeding 150 $\mu$A were used. The stimulating current was monitored on the oscilloscope using a 100 Ω resistor connected in series with the stimulating micro-electrode.

The right vagus nerve was stimulated electrically through a bipolar, platinum electrode placed low in the neck. The distance from the electrode to the ganglion was 40–62 mm. The stimulus intensity did not exceed eight times the threshold required to evoke a field potential in the nodose ganglion.

*Experimental protocol*

Each experiment entailed the study of the central projections of a single afferent cell. We first determined the location of the dorsal respiratory group in the ventrolateral subnucleus of the n.t.s. by recording from inspiratory neurones with the steel micro-electrode. Starting lateral to the sulcus intermediolateralis, we systematically searched at a single rostrocaudal level (1·0–1·5 mm rostral to the obex), in 0·2 mm steps, for a locus where strong, spontaneous, multi-unit activity time-locked to the phrenic inspiratory discharge could be recorded. The micro-electrode was then left in this location.

Following this, we searched for r.a.r. neurones in the nodose ganglion by recording single-unit

activity. Because many r.a.r. neurones of the cat are inactive at eupnoeic tidal volumes (Paintal, 1973), the ganglion was explored during continuous, 1 Hz, stimulation of the vagus nerve. We tested each cell excited by vagal stimulation for characteristic properties of r.a.r.s (Widdicombe, 1954). Identification of an r.a.r. was based principally on the presence of a rapid adaptation (greater than 70% within 2 s from the peak firing rate) to a fast rising, then maintained ('ramp and hold'), hyperinflation of the lung (peak volume = 100–140 ml, about 3 times control tidal volume; air flow = 3·6–6·4 l/min, about 3 times control air flow).

The antidromic mapping *per se* began in the track where the dorsal respiratory group neurones were located. This enabled us to verify, at the very beginning of the mapping session, that the axon of the cell under study reached the solitary tract (using strong stimuli) and to make a preliminary assessment of the projection and branching within the region of inspiratory cells (using weaker stimuli). Because in the earliest experiments we found that r.a.r. neurones project to the contralateral n.t.s., we next searched for the location of distal branches on that side. This avoided damage to be ipsilateral branches before their distal portions were studied. The spacing between penetrations was 0·2–0·4 mm. Since we wanted to determine both the over-all extent of the projection and the course of individual branches, and this had to be achieved within the period that the preparation remained stable, the final distribution of the points of penetrations did not conform to a systematic grid (cf. Fig. 2).

In each penetration, the stimulating micro-electrode was advanced until antidromic activation was achieved with a current of 150 $\mu$A. Then the penetration was continued in fixed steps of 100 $\mu$m, or 50 $\mu$m in those loci where the threshold intensity was below 20 $\mu$A. At each site, changes in the latency of the response were also assessed as the stimulus intensity was varied between 0 and 150 $\mu$A (see Results for details). Since in some penetrations antidromic responses having up to nine distinct latencies could be evoked at different stimulus intensities, the collision test was used to confirm that each response of different latency resulted from stimulation of a branch of the r.a.r. under study. The thresholds and latencies were determined with an accuracy of 10% and 0·05 ms, respectively.

In seven experiments, after the mapping was completed, the chest was opened and the pulmonary location of the receptive field of the r.a.r. verified by local, mechanical probing of the lung.

At the end of the experiment, a single site containing branches of the r.a.r. under study was marked by passing a 15 $\mu$A current (tip positive) for 30 s through the stimulating micro-electrode to deposit ferric ions. The cat was then perfused with 10% formalin in saline containing 5% potassium ferrocyanide to obtain a Prussian blue spot (Green, 1958). Subsequently, serial, transverse sections of the medulla, 50 $\mu$m thick, were cut on a freezing microtome, stained with neutral red and mounted for examination.

*Analysis of the depth–threshold curves*

The basic data obtained from each antidromic mapping session consisted of records of threshold currents and corresponding response latencies together with the position of the stimulating micro-electrode. For each penetration and distinct response, a plot of electrode depth against threshold current can be drawn (depth–threshold curve; see Fig. 2). The steepness of the depth–threshold curve is a measure of the spatial resolution of the technique and allows one to estimate the distance between the micro-electrode and the stimulated fibre (Ranck, 1975; Lipski, 1981).

As expected from earlier studies (Armstrong, Harvey & Schild, 1973; Merrill, 1974; Shinoda, Arnold & Asanuma, 1976; Marcus, Zarzecki & Asanuma, 1979; Hentall, Zorman, Kansky & Fields, 1984), most of the depth–threshold curves had their data points distributed fairly symmetrically about a minimum and suggested a parabolic rather than a linear relationship (see Results for details). The variability in the steepness of different curves (relating to different branches) was so great that it did not seem appropriate to apply the same estimate of current spread to all penetrations.

Therefore, to evaluate the current spread, we determined the steepness of each depth–threshold curve by fitting a parabola to the data for the individual penetrations. Several earlier studies had shown that depth–threshold curves can be expressed mathematically by the equation

$$I_{th} = Ad^2 + I_0, \quad (1)$$

where $d$ is the depth of stimulation (measured from the minimum threshold point), $I_{th}$ is the

threshold current, and $A$ and $I_0$ are coefficients (Armstrong *et al.* 1973; Merrill, 1974; Marcus *et al.* 1979). The coefficient $A$ depends on the fibre type and specific impedance of the tissue (BeMent & Ranck, 1969; Jankowska & Roberts, 1972; Roberts & Smith, 1973; Gustafsson & Jankowska, 1976; Shinoda *et al.* 1976). It does not depend on the angle between the fibre course and the direction of penetration if the site of excitation of the fibre remains unchanged throughout the penetration. (The $A$ coefficient also may depend on the electrode tip geometry and/or stimulus shape and duration, but there are no data suggesting the nature of this dependence; since the micro-electrode tip was at least an order of magnitude smaller than the distances involved and the stimulus duration was short (0·1 ms), we neglected these factors.) The $I_0$ coefficient is proportional to the minimum distance ($r_{min}$) between the stimulated fibre and the micro-electrode tip and the absolute minimum ($I_{min}$) threshold which one can measure when the micro-electrode touches the fibre at one of the nodes of Ranvier (Jankowska & Roberts, 1972). On the basis of eqn. (1), $I_0$ may be expressed as:

$$I_0 = Ar_{min}^2 + I_{min}. \tag{2}$$

In the present study, in an attempt to obtain a practicable measure of the current spread, we fitted parabolic equations to all depth–threshold graphs that contained at least 4 points and did not show any sharp discontinuities that would suggest an uneven penetration of the electrode. Since in our experiments we did not systematically search for a minimum threshold point in each penetration, our graphs were interpolated by the equation:

$$I_{th} = Ad^2 + Bd + C, \tag{3}$$

where $A$ is the same coefficient as in eqn. (1), while $B$ and $C$ determine the location of the minimum on the curve. The interpolations (as well as all regression analyses) were performed on a Tektronix 4051 minicomputer equipped with a 'Plot 50' statistics program. By neglecting the variability in tissue impedance and by assuming that a fixed latency of the response indicates that the fibre is activated at the same locus (node of Ranvier) throughout the penetration, we could regard the $A$ coefficient as a measure of the effective current spread that is characteristic of the fibre. Furthermore, since $I_{min}$ is less than 1 $\mu$A (the lowest threshold ever found in the present study was 0·94 $\mu$A), we felt that for the depth–threshold curves having $I_0$ higher than 10 $\mu$A, $I_{min}$ could be assumed to be zero. This last assumption allowed us to use eqn. (2) to evaluate the distance between the minimum threshold point and the stimulated fibre (once the $A$ coefficient was determined from the eqn. (3)):

$$r_{min} = (I_0/A)^{0.5} \tag{4}$$

Thus, the $A$ coefficient was used to estimate the effective current spread, evaluate the spatial resolution of the method, and assess the relationship between the steepness of the depth–threshold curve and the conduction velocity of the stimulated fibre (see Results).

*Reconstruction of the central projection*

The actual location of each penetration was determined on the basis of its coordinates with respect to the obex, the location of the Prussian blue mark and inspection of the serial sections of the medulla. Since the micro-electrodes that we used left noticeable tracks on the sections, we could determine the actual location of most penetrations despite the limited accuracy ($\pm 50$ $\mu$m) of the stereotaxic coordinate readings and the occurrence of tissue displacements in regions of dense tracking. The position of each penetration was then superimposed on a corresponding camera lucida drawing of a transverse section. The location of each track was also plotted on a map showing a dorsal view of the medial and lateral borders of the n.t.s.; this map was drawn for each experiment from measurements taken from the serial sections. The medullary course of each r.a.r. axon and its major collaterals within the n.t.s. was deduced from: (1) the latency of the antidromic response at each low-threshold point, (2) an estimate of the conduction velocity along a supposed course of a given branch, and (3) the location of the minima on depth–threshold curves determined for each antidromic response characterized by a distinct latency combined with the estimate of the distance of the fibre from the electrode based on the $A$ coefficient analysis, as outlined in the preceding section.

## RESULTS

### *General properties of r.a.r.s studied*

Eleven receptor cells for which maps of their central projections were obtained were identified as r.a.r.s on the basis of a rapid adaptation of their firing rate to ' ramp and hold ' lung inflations. One of these, although characterized as an r.a.r. on the basis of its rapid adaptation, had a very regular and highly repeatable firing pattern following hyperinflation, uncharacteristic of r.a.r.s (Widdicombe, 1954). The central projection pattern of this cell was also significantly different from all the others and will be treated separately.

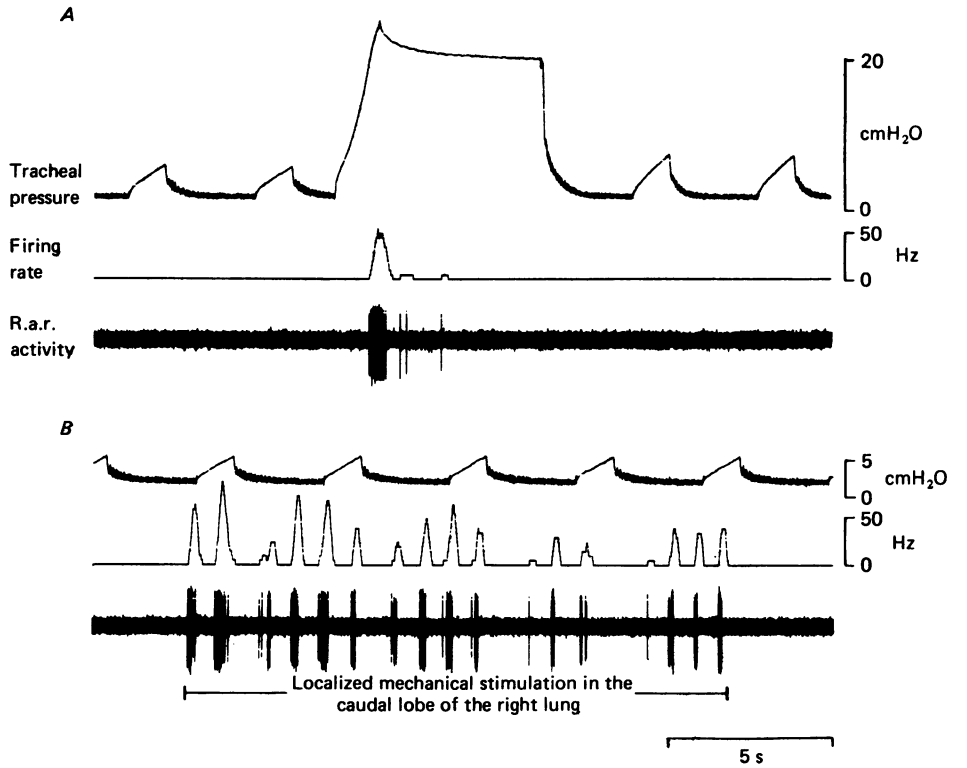


Fig. 1. Identification of r.a.r. cell (*A*) and response to local mechanical stimulation (*B*). Note the rapid onset and adaptation of the cell's firing in response to hyperinflation of the lungs. The cell was silent at eupnoeic tidal volumes. In *B*, the dorsolateral aspect of the caudal lung lobe was mechanically stimulated with a glass probe. Each burst of action potentials represents a response to one touch. The apparent modulation of the strength of the response with the frequency of ventilation resulted from a decreased stimulus strength during lung expansion. This is r.a.r. No. 27 in Table 1.

Although our criterion was an adaptation of the firing rate greater than 70 % within 2 s from the peak, in fact, all the cells had an adaptation index of 90–100 %. All were silent at eupnoeic tidal volumes (e.g. Fig. 1 *A*). The threshold pressure at which firing was initiated was 1·3 (cell No. 21)–3·0 (cell No. 13) times the pressure at the peak of the eupnoeic tidal volume. In some cells, we observed an irregular, low-frequency

TABLE 1. Properties of the r.a.r. cells whose central projections were mapped

| | Firing threshold for lung inflation | | | Conduction velocity (m/s) | |
|---|---|---|---|---|---|
| Cell No. | Tracheal pressure ($cmH_2O$) | Volume (ml) | Receptor location (lung lobe) | Vagal (without temperature correction) | Main axon within t.s. ±S.E. |
| 9 | 13·7 | N.d. | N.d. | 15·6 | N.d. |
| 10 | 11·5 | 99 | N.d. | 14·7 | N.d. |
| 13 | 11·4 | 88 | N.d. | 15·8 | 7·5±2·0 |
| 18 | 11·2 | 67 | Caudal | 17·1 | 6·2±0·7 |
| 19 | 14·2 | N.d. | N.d. | 15·4 | 6·5±1·1 |
| 21 | 5·2 | 37 | Cranial | 20·4 | 7·9±1·0 |
| 22 | 13·0 | 89 | Caudal | 19·3 | 9·7±1·3 |
| 25 | 21·5 | 107 | Cranial | 11·2 | 7·3±0·4 |
| 27 | 19·0 | 113 | Caudal | 18·5 | 9·7±0·4 |
| 29 | 23·0 | 103 | Not found | 14·8 | 7·5±1·8 |
| 30 | 20·8 | 110 | Caudal | 13·7 | N.d. |

N.d. = not determined.

discharge when the expiratory load was briefly removed. This spontaneous firing pattern clearly differed from that evoked by mechanical probing of the surface of the lung in the region where the receptor was located. This latter response was a high-frequency burst of action potentials occurring in response to each touch (e.g. Fig. 1*B*). The mechanical thresholds for local probing were sufficiently low to assume that the receptive area was located close to the probe. Table 1 summarizes some of the properties of the r.a.r. cells whose central projections were investigated.

Besides the r.a.r. cells whose central projections were mapped, we studied an additional thirty-five r.a.r. and thirty p.s.r. neurones. The average vagal conduction velocity for r.a.r.s, 15 m/s±3 (S.D.) ($n = 46$), was significantly lower than that for p.s.r.s, 24 m/s±9 ($n = 30$) ($P < 0{\cdot}005$). This indicates that, despite a substantial overlap in the distribution of the conduction velocities, the afferent fibres from r.a.r.s were considerably thinner than those from p.s.r.s. It was our impression that the micro-electrode tip had to be smaller for r.a.r. than for p.s.r. recordings in order to obtain a satisfactory signal-to-noise ratio. This is consistent with the observed difference in conduction velocities and suggests that the cell bodies of r.a.r.s are, on average, smaller than those of p.s.r.s. The r.a.r. cells for which maps of the central projections were obtained had an average conduction velocity of 16 m/s±3 (S.D.), close to that of the total population of forty-six r.a.r.s.

*Types of depth–threshold curves*

The depth–threshold data for individual penetrations fit into four groups. Typical examples are shown in Fig. 2 which shows the distribution of stimulation points within the n.t.s. in one experiment, as seen in a dorsal view of the medulla.

(*1*) *A simple curve of parabolic shape* (*e.g. Fig. 2A*). These were obtained from those penetrations in which the response had a constant latency at every depth. The curves were usually symmetrical around the point of a minimum threshold. They were

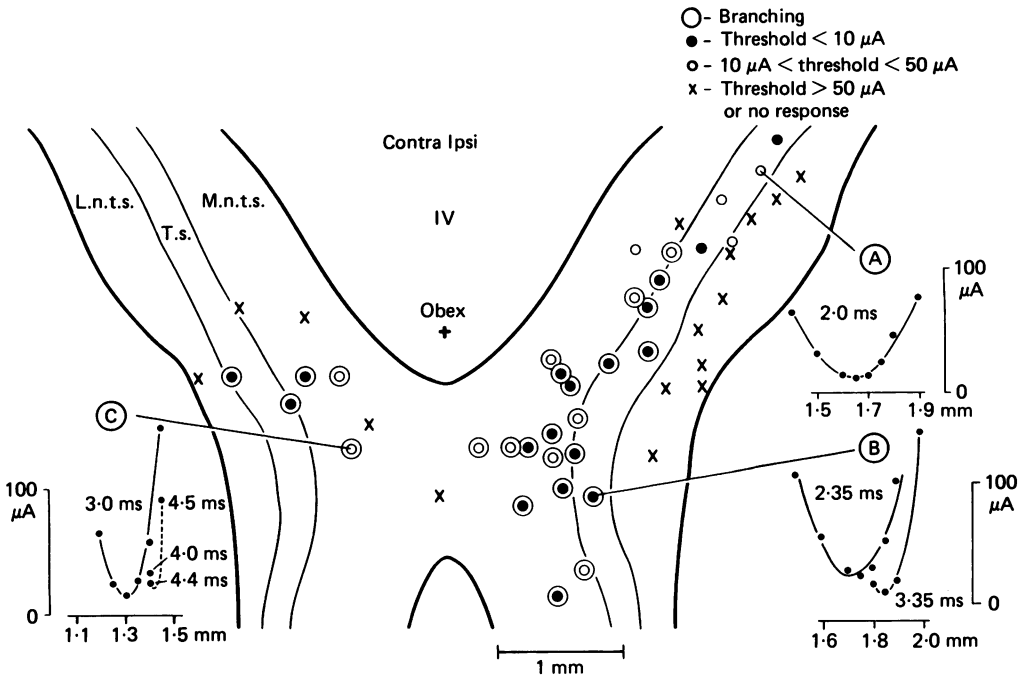


Fig. 2. Examples of depth–threshold curves obtained in one mapping session from different n.t.s. regions. As seen in a dorsal view, the heavy lines show the borders of the n.t.s. and the thin lines the course of the t.s. which divides the nucleus into its medial (m.n.t.s.) and lateral (l.n.t.s.) portions (m.n.t.s. and l.n.t.s. in this and subsequent Figures). Each symbol corresponds to one penetration throughout the depth of the nucleus. Circled symbols indicate tracks from which responses with at least two different latencies could be evoked (multiple branches). Insets *A*, *B* and *C* show examples of depth–threshold curves obtained from three penetrations (the depth was measured from the dorsal medullary surface). The continuous lines represent the best fitting parabolas found for points corresponding to a single response characterized by a distinct latency. The dashed line in *C* connects two points which could correspond to stimulation of the same, particularly thin, branch. The latencies of the responses are indicated next to the curves. Data from r.a.r. No. 21.

interpreted as resulting from stimulating a single central branch of the mapped cell at a fixed point along its course.

(*2*) *Multiple curves of parabolic shape* (*e.g. Fig. 2B*). In some loci, a stimulus of relatively low intensity evoked a spike characterized by a well defined threshold and a constant latency; then, as the intensity was increased, a response with a different (usually shorter) latency was evoked and the lower threshold one was no longer present. This new response was also characterized by a well defined threshold and a constant latency. Such double latencies were interpreted as being due to stimulation of two distinct branches that differed in their conduction distance and/or velocity along the pathway to the ganglion. In many cases, plots of the depth–threshold curves could be interpolated by two distinct parabolas.

In some penetrations, at some points of stimulation in which two latencies were encountered, a continuous decrease in latency, rather than a sudden 'jump', was

observed as the stimulus intensity was gradually increased. In such instances, we assumed that the stimulating current spread gradually from a thin collateral located relatively close to the tip of the stimulating electrode toward a parent branch located more distally from the electrode.

In fact, in many penetrations, more than two distinct responses characterized by different latencies could be evoked, indicating more than two branches in the vicinity of the electrode tip. If, on the basis of minimum threshold currents, we determined that several branches were located within a radius of 0·2 mm, we referred to such sites as branching points (see Fig. 2, circled symbols).

(*3*) *Scattered points on the depth–threshold graph* (*e.g. Fig. 2C*). In some penetrations, responses of particularly long latencies could be evoked from isolated points in the track. These were evoked either alone or in conjunction with several responses with distinct latencies for which corresponding depth–threshold curves could be determined. These long latencies were most often in the range of 4·0–18·0 ms, compared to the typical range of 2·5–3·5 ms. The collision test confirmed that these responses were evoked from branches of the r.a.r. cell recorded in the nodose ganglion. Thus, we assumed that they were evoked in particularly thin, slow conducting, possibly terminal branches. The responses were also quite susceptible to the anodal surround effect (see Ranck, 1975; Lipski, 1981); that is, they were often blocked by stimulation with currents about twice the threshold. For six such responses we determined the thresholds every 20–50 $\mu$m regardless of the threshold encountered and were able to demonstrate smooth, very steep, parabolic depth–threshold curves (range of $A$ coefficients: 5700–18750 $\mu A/mm^2$). Thus, it seems that these responses were only quantitatively different from those dealt with in the two preceding sections.

(*4*) *Asymmetrical depth–threshold curves.* Depth–threshold curves which clearly deviated from a symmetrical, parabolic shape were observed when a change in the depth of stimulation was associated not only with a change in threshold but also with a systematic shift in the latency of the response. These curve patterns were interpreted as being due to the advancement of the stimulating electrode in parallel with the course of the stimulated fibre and to a shift in the excitation site as the electrode was advanced. The conduction velocity of the fibre was sufficiently low to allow for a noticeable change in the latency of the response over several tenths of a millimetre.

The only other instances when the depth–threshold curves were clearly asymmetrical were those in which the tissue was compressed by the downward movement of the stimulating electrode. In these cases, the response latencies were recorded but further penetration was discontinued. The latency of response taken in such instances was usually helpful in interpreting the data from other, neighbouring, penetrations.

*Steepness of the depth–threshold curves*

320 depth–threshold curves that fulfilled the criteria outlined in the Methods were selected for interpolation by eqn. (3). Of these, 84 % consisted of five to fourteen experimental points, and 80 % displayed a minimum threshold below 50 $\mu$A. The correlation coefficients for the fitted curves were better than 0·9 in 93 % of cases and between 0·8 and 0·9 in the remainder.

The resulting $A$ coefficients ranged from 400 to 18750 $\mu A/mm^2$. The range in the

pooled data was similar to that observed in individual experiments. Since r.a.r. fibres have such a wide range of values of the $A$ coefficient, use of a single estimate of the effective current spread for all branches of an individual neurone could lead to substantial errors. Instead, the value of the $A$ coefficient was used to estimate the current spread. By using eqn. (4), one can find, for example, that a stimulus current of 10 $\mu$A could excite a fibre having an $A$ coefficient of 400 if it lies within a radius of 158 $\mu$m from the electrode tip, whereas the same current would excite a fibre having an $A$ coefficient of 18750 $\mu$A/mm$^2$ only if the electrode tip is less than 23 $\mu$m from the fibre. In addition, determination of the $A$ coefficient provided quantitative information on the conduction velocity of the stimulated fibre (see the next section).

*Relationship between the conduction velocity and the steepness of the depth–threshold curve*

*Qualitative observations.* It has been shown that the shape of the depth–threshold curve depends on the conduction velocity of the stimulated fibre; the lower the conduction velocity, the steeper the curve (BeMent & Ranck, 1969; Jankowska & Roberts, 1972; Roberts & Smith, 1973; Gustafsson & Jankowska, 1976; Shinoda *et al.* 1976). These earlier studies dealt, however, with fibres having conduction velocities much greater than those of central branches of r.a.r.s. Only BeMent & Ranck (1969) attempted a quantitative assessment of the relationship between the conduction velocity and the steepness of the corresponding depth–threshold curve.

In the present study, three types of evidence confirmed an inverse relationship between the conduction velocity and the steepness ($A$ coefficient) of the depth–threshold curve. First, the depth–threshold curves obtained from the regions of r.a.r. projection in which a significant tapering of central branches could be expected (e.g. contralateral n.t.s.) were always steeper than those found for the main axon in the ipsilateral n.t.s. (cf. Fig. 2$A$ and $C$). The range of $A$ coefficients found for the main axons of r.a.r. cells was 400–1400 $\mu$A/mm$^2$, while that for distal branches (based on their location and response latencies) was 1760–18750 $\mu$A/mm$^2$. Secondly, in individual penetrations in which two or more branches having substantial differences in their antidromic response latencies were stimulated, the depth–threshold curve of the branch having the longer response latency characteristically had a higher $A$ coefficient (e.g. Fig. 2$B$). Although in most instances we were unable to determine the actual conduction distances to the ganglion, when the difference in latency was greater than 1 ms it seemed reasonable to assume that at least part of the difference was due to different conduction velocities.

Finally, for nine r.a.r. cells we drew propagation distance–antidromic latency graphs for intramedullary portions of their main axons and some major collaterals. Such graphs allow one to estimate the conduction velocity along a selected portion of the fibre (Jankowska & Roberts, 1972). By plotting the $A$ coefficient values obtained for the corresponding portions of the fibres on the same coordinates, we could see a correlation between the conduction velocity and the $A$ coefficient. Fig. 3 shows the relationship between the propagation distance and both the antidromic latency and the $A$ coefficient of the main axon and two collaterals of a single r.a.r. cell. (The course of major collaterals within the n.t.s. is shown for this cell in Fig. 5.) The distance–latency graph is given by the open symbols. The seven points at which the main axon was stimulated are distributed along a straight line, indicating a constant

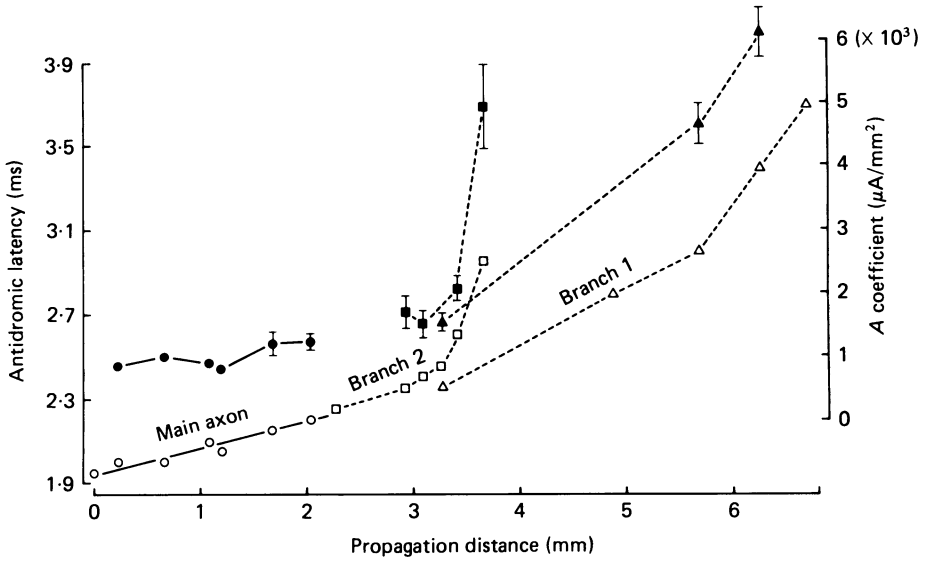


Fig. 3. Propagation distance–antidromic latency and propagation distance–*A* coefficient graphs for the main axons (circles) and its two major collaterals (branch 1: triangles; branch 2: squares; cf. Fig. 5). The distance–*A* coefficient graphs are those having filled symbols (scale on the right-hand side). The distance was measured along the supposed course of each branch from the most rostral penetration in which the main axon was stimulated. In a few penetrations, only the latency value could be obtained; thus some points on the distance–latency graphs do not have corresponding points on the distance–*A* coefficient curves. For further explanation, see text.

conduction velocity along the main axon at levels rostral to the obex (continuous line, ○). The conduction velocity evaluated for this portion of the axon by linear regression was 7·9 m/s ± 1·0 (S.E.) ($r$ = 0·925). Then, beyond the point where the main axon divided into branches 1 and 2, the distance–latency plots (dashed lines, △ and □, respectively) become non-linear. This suggests a decrease in the diameter of the fibre, most pronounced in the terminal portions of these branches. The *A* coefficient for the main axon is fairly constant (795–1230 μA/mm², continuous line, ●). This is consistent with the constant conduction velocity indicated by the distance–latency plot. In contrast, the *A* coefficients for both branches 1 and 2 increase non-linearly toward the distal portions (dashed lines, ▲ and ■, respectively). Since the corresponding distance–latency graphs are also non-linear and indicate a substantial decrease in conduction velocity, these data taken together suggest that the value of the *A* coefficient may yield useful, quantitative information about the conduction velocity of the stimulated branch.

*Quantitative analysis.* Although a number of authors have suggested that the steepness of the depth–threshold curve is inversely related to the conduction velocity ($v$), only a few have reported the actual values of $v$ together with the corresponding data on the shapes of depth–threshold curves. The following were found: Jankowska & Roberts, 1972, Fig. 6: $v$ = 85, 70 and 9 m/s; Jankowska & Smith, 1973, Fig. 4*A*, widest curve: $v$ = 30 m/s (personal communication); Roberts & Smith, 1973, Fig. 3: $v$ = 67 and 60 m/s; Merrill, 1974, Fig. 19·6: $v$ = 38 m/s; Morrison & Gebber, 1985,

Fig. 11, portion of curve 'A': $v \approx 2{\cdot}2$ m/s. The corresponding $A$ coefficients were obtained by measuring coordinates of three points on the published figures and interpolating the data by a parabolic equation. Merrill (1974) reports the value of the $A$ coefficient directly, and the corresponding conduction velocity was subsequently given by Gustafsson & Jankowska (1976). A plot of the $A$ coefficients against $v$ on a log–log scale for these published data suggested a linear relationship (Fig. 4). To those points we added seven pairs of $A$–$v$ values from the present study. The data were obtained from main axons or major collaterals for which we determined at least four points on the distance–latency graphs, together with the corresponding $A$ values, and that had a uniform conduction velocity over the portion analysed. Our data (●), which covered the range 5·0–9·7 m/s (Table 1), fall within the area of the graph in

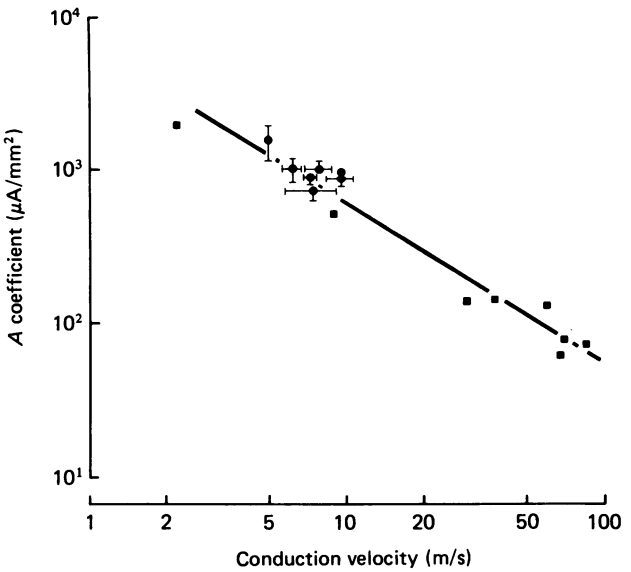


Fig. 4. Relationship between the $A$ coefficient (steepness of the depth–threshold curve) and the conduction velocity of the fibre. ■, points obtained by recalculation of data from previous studies, as listed in the text. ●, our data based on stimulation of major collaterals of r.a.r. cells. Lack of S.E. bars indicates that the errors were smaller than the size of the symbol. The continuous line was obtained by linear regression through all the data points.

Fig. 4 expected by a linear interpolation of the data from the other studies (■) and were also distributed in a manner consistent with an inverse relationship between the $A$ coefficient and $v$. Therefore, the assumption of a linear relationship (on a log–log scale) between the two parameters appeared reasonable. The regression line drawn to include all the data points (heavy line) was described by the equation: $\log A = a \log (v) + b$ ($r = 0{\cdot}951$), where $a = -1{\cdot}03 \pm 0{\cdot}06$ (S.E.) and $b = 3{\cdot}81 \pm 0{\cdot}08$ (S.E.). Extrapolation along this line allows one to evaluate the conduction velocity in fine branches for which a direct measurement of their conduction velocity is not possible due to either their short length or complicated course. For example, one can find that depth–threshold curves having an $A$ coefficient of 3000 $\mu$A/mm$^2$ should result from stimulation of branches having a conduction velocity of 2·1 m/s (the $\pm 3$ S.E. limits give a 1·2–4·7 m/s range).

In the present study, 58 of the 320 depth–threshold curves had $A$ coefficients between 3000 and 18750 $\mu A/mm^2$. Moreover, we found numerous long-latency responses for which full depth–threshold curves could not be obtained; these long latencies presumably represented slow conduction in very thin fibres whose $A$ coefficients would be about 10000 $\mu A/mm^2$. Although it may be too crude an extrapolation to derive exact values for the conduction velocity from our linear regression equation for $A$ values higher than about 3000 $\mu A/mm^2$ because of the possibility of large errors within that range (see Discussion), the analysis suggests that the thinest branches stimulated in the present study had conduction velocities below 1 m/s. This indicates that in many instances we stimulated portions of fibres that may be non-myelinated and located close to the terminals.

The quantitative knowledge of the $A$–$v$ relationship was quite useful for reconstructing the projection of r.a.r.s. For example, during stimulation relatively close to the main axon, in several instances we recorded responses with latencies equal to, or slightly longer than, those of the main axon; however, the depth–threshold curves for those responses had $A$ coefficients four times greater than that of the main axon in the adjacent regions. Thus, knowledge of the $A$–$v$ relationship allowed us to conclude with satisfactory confidence that the fibres with high $A$ coefficients represented thin branches of the main axon rather than the main axon itself.

*Central course of the main axon and major collaterals*

Based on the latencies of responses evoked from regions rostral to the obex, it was possible to localize the main axon of each r.a.r. cell unequivocally. The most rostral level at which the axon was localized was determined by the exposure of the medulla and varied from 1·15 to 2·3 mm rostral to the obex. The shortest latencies of responses evoked from such rostral points varied from 1·85 to 3·1 ms. At these rostral levels the axons of all cells were within the tractus solitarius (t.s.).

The course of the main axon along the t.s. was traced on the basis of a systematically increasing latency of the response. Fig. 5 shows an example of the distribution of response latencies and lowest thresholds obtained from penetrations in which the main axon or its major collaterals were stimulated. The data shown here are for the same r.a.r. as that illustrated in Fig. 2. The correctness of attributing individual response latencies to stimulation of the same branch at different levels was further verified by plotting propagation distance–antidromic latency graphs, as illustrated earlier for this cell in Fig. 3 (open symbols).

In a similar manner, the course of the main axon within the t.s. was traced over a length of 0·9–3·0 mm for eight other cells (see Table 1). Typically, at levels just caudal to the obex, the main axon divided into at least two major branches. The most common pattern of ramification was that of one branch turning medially and reaching the contralateral nucleus and another continuing in parallel to the ipsilateral t.s., to 1·3–2·2 mm caudal to the obex (see two other typical examples in Fig. 7*B* and *C*).

*Distribution of the terminal branches of r.a.r.*

It was not possible to reconstruct the detailed course of branches of an order higher than the major collaterals (and not all of these) (cf. Jankowska & Roberts, 1972). The difficulty stemmed from the short length and possibly complicated course of the

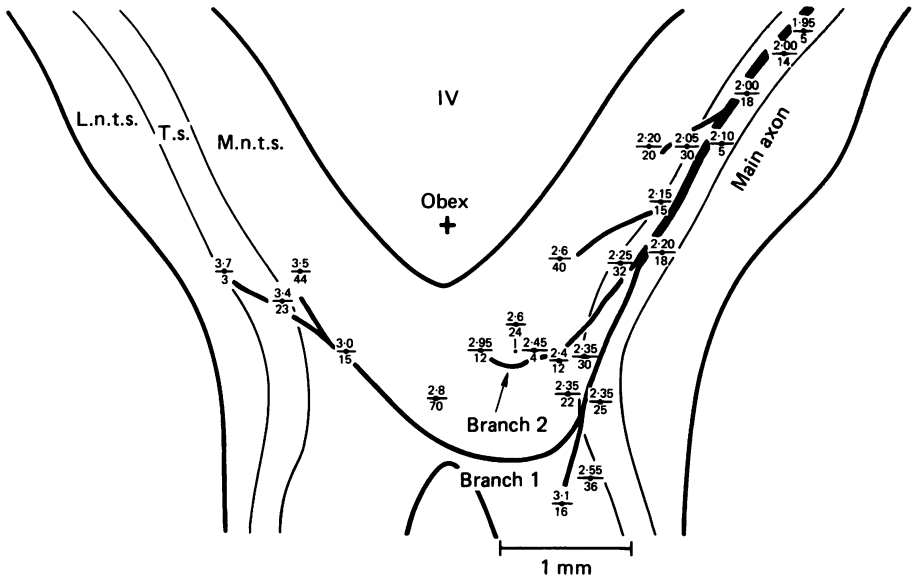


Fig. 5. Course of the main axon and major collaterals of one r.a.r. cell (same as in Figs. 2 and 6). The latencies (numerator, ms) and lowest thresholds (demoninator, $\mu$A) are shown at points of penetrations placed along the course of the branches.

fine branches and the high density of branching in some regions. The very steep depth–threshold curves of fine branches required that penetrations be spaced closer than 50 $\mu$m to trace a single branch in detail. On the other hand, a picture such as Fig. 2 does not represent the location and density of fine branches in different n.t.s. regions with satisfactory detail.

Accordingly, the relative density of fine branches in different n.t.s. regions was represented in a semi-schematic fashion. Each response that could not be attributed to stimulation of a major collateral was regarded as being evoked in a separate fine branch. The fine branches so defined were then drawn as thin bars branching off from major collaterals in such a way that their location and suggested point of insertion on major collaterals or lower order branches were not in conflict with data obtained from other penetrations close to the analysed point (threshold, latency, depth, $A$ coefficient). Where available, the data on 'jumps' or continuous changes in the latency with increasing stimulus intensity were used according to the interpretation previously given.

Fig. 6$A$ shows the distribution of fine branches for the r.a.r. cell whose major collaterals were drawn in Fig. 5. Although the course of the fine branches is schematic, Fig. 6$A$ does show the exact number and approximate location of such branches that we found in the different n.t.s. regions. The fine branches were localized almost exclusively to the medial and caudal portion of the ipsi- and contralateral n.t.s. The shaded circles indicate those regions in which no collaterals of this r.a.r. cell could be detected. The diameters of the individual circles were determined from the maximum subthreshold current (or 100 $\mu$A, whichever was lower) for a given penetration by application of eqn. (4) and using the largest $A$ coefficient found for the main axon or a major collateral located in or close to the negative penetration.

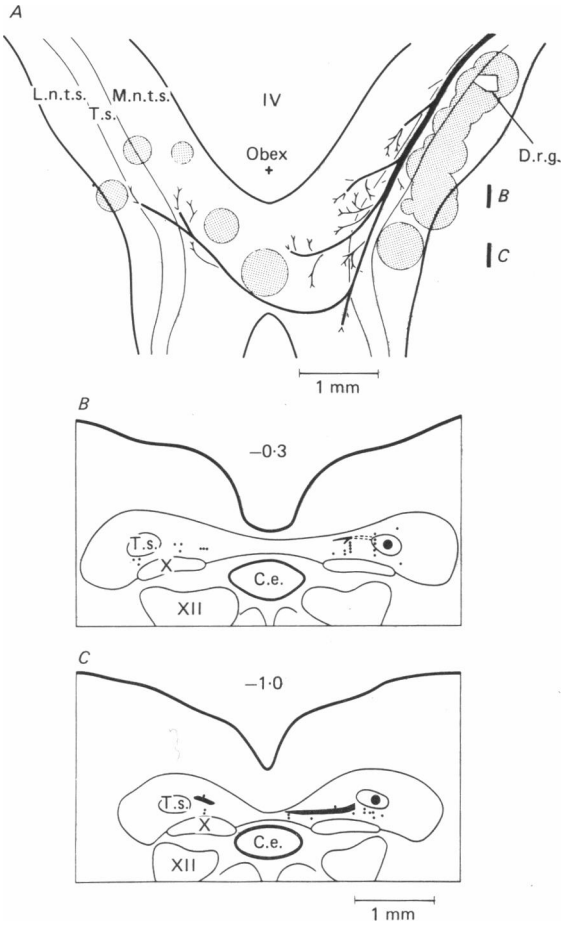


Fig. 6. Schematic distribution (see text) within the n.t.s. of fine branches of the same r.a.r. cell as in Figs. 2 and 5. In *A*, the branching pattern is shown in a dorsal view. The stippled circles cover the regions in which presence of branches was excluded on the basis of current spread analysis. The white area in the upper right portion of the shading indicates the region in which inspiratory cells (d.r.g.: dorsal respiratory group) were recorded. *B* and *C* show two coronal sections on which the location of fine branches is indicated by small dots. Each drawing shows branches contained in a 0·3 mm thick medullary segment located at the level indicated by heavy bars in *A*. The main axon is shown as a heavy filled circle within the t.s. on the right side. The continuous lines correspond to portions of major collaterals that course within the plane of the section. The small dots are located at the depth of the minimum threshold current to activate the fine branches. Most fine branches were located in the intermediate, medial and commissural subnuclei of the n.t.s. Abbreviations: c.e., central canal; t.s., solitary tract; X, dorsal motor nucleus of the vagus nerve; XII, hypoglossal nucleus.

Due to steeper depth–threshold curves for finer branches, regions containing relatively thin fibres required denser penetrations in order to surround identified collaterals with 'no projection' circles.

Fig. 6*B* and *C* shows the location of major collaterals and fine branches in the transverse plane at two levels caudal to the obex. The portions of the major collaterals

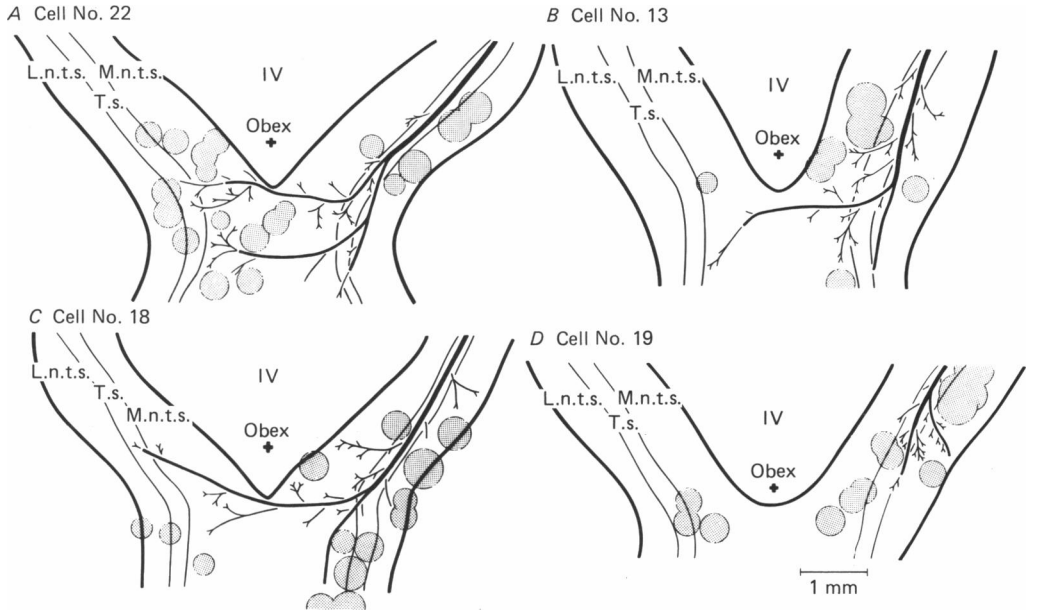


Fig. 7. Examples of branching patterns of four cells. *A*, *B*, and *C* show patterns typical for the population of r.a.r.s studied, with the greatest concentration of fine branches occurring medial to the t.s., just caudal to the obex. Each cell has at least one major collateral reaching the contralateral nucleus and one descending ipsilaterally along the t.s. In *D*, the branching pattern of the one cell that displayed only an ipsilateral projection, mostly confined to the ventrolateral n.t.s., is drawn. The stippled areas in all drawings indicate the regions where the presence of branches could be excluded.

that passed within the plane of section are shown as continuous lines while each small dot corresponds to one fine branch and is located at the depth of the minimum current for that branch. Most fine branches were localized in the ventral and medial portion of the n.t.s., just below and medial to the t.s.

In Fig. 7*A*, *B* and *C*, reconstructions for three additional cells, typical of the r.a.r. population, are given. Here again, the densest branching was detected in the caudal, medial portion of the ipsi- and contralateral n.t.s. The cells in Fig. 7*B* and *C* also had a few collaterals in the dorsolateral and ventrolateral n.t.s., respectively. All ten r.a.r. cells displayed the densest branching in the medial n.t.s., caudal to the obex. This region coincides with the caudal portion of the medial and commissural subnuclei of the n.t.s. (Loewy & Burton, 1978; Kalia & Mesulam, 1980). Nine cells had some branches in the corresponding region of the contralateral n.t.s. (in one cell it was not adequately tested). All cells also had a few branches in the medial n.t.s. rostral to the obex. In six r.a.r.s, at least one branch extended lateral to the t.s. In three of those, the lowest threshold points were located dorsal to the t.s., while the other three cells had some branches within the ventrolateral n.t.s. at sites where we recorded inspiratory cell activity. For six r.a.r.s, low-threshold points were located in, or very close to, a region located right under the t.s. just caudal to the obex (cf. Fig 6*B* and *C*). This region, interposed between the medial and ventrolateral n.t.s., is referred to as the intermediate nucleus (Loewy & Burton, 1978; Kalia & Mesulam, 1980). The

area of the r.a.r. projection, as seen in a dorsal view, was determined from the maps. It averaged 2·4 $mm^2 \pm 0{\cdot}4$ (S.D.); of that, $22\% \pm 9$ was contralateral.

Stimulation in the ipsilateral, medial part of the n.t.s., rostral to the obex revealed another interesting feature of the projection of r.a.r.s. Responses having rather long latencies (4·1–8·3 ms), could be evoked only from isolated points along the electrode track, and only with relatively high currents (70–120 $\mu$A). Rarely were responses having latencies intermediate between these very long ones and those ascribed to the main axon evoked. Thus, it seems likely that the structure of fine branches in the medial n.t.s. rostral to the obex differs from that in the remaining projection area. The features of the responses suggested that they were evoked in long, thin branches that originated from major collaterals (possibly the main axon) coursing some distance from the rostral part of the medial n.t.s. Since the actual points of origin and course (possibly complicated) of such branches could not be determined, they could not be distinguished graphically from other fine branches on the schematized drawings of branching patterns.

*R.a.r. cell with atypical branching pattern*

One cell, classified as r.a.r. on the basis of its adaptation index to lung inflation, displayed a central projection pattern significantly different from the rest of the population studied (Fig. 7*D*, cell No. 19); the central projection was limited to the ipsilateral medial, lateral and ventrolateral n.t.s., with the latter projection being most pronounced. This cell had an extremely regular and repeatable firing pattern in response to lung inflations. This firing pattern, together with the pattern of projection, suggested the possibility that the cell was, in fact, an extreme example of a p.s.r. with a high threshold and high dynamic sensitivity. Therefore, we think that the projection pattern of this cell should not be regarded as representative of r.a.r. cells; indeed, it resembled that of a p.s.r. cell (see next section).

*Comparison with central projection of p.s.r.*

The contralateral projection of r.a.r.s contrasted with the absence of such projections in p.s.r.s (Donoghue *et al.* 1982; Berger & Averill, 1983). In view of the different protocol that we used, especially our use of closely spaced penetrations to trace fine branches, we decided to reassess the possibility that p.s.r.s do project to the contralateral n.t.s. Two p.s.r. cells were studied. Both had low volume thresholds and a continuous, regular activity that increased during each lung inflation. During 'ramp and hold' inflation tests (cf. Fig. 1), their firing rate followed the changes in tracheal pressure and showed little adaptation (adaptation indices lower than 16%). After verifying, by antidromic activation, that the cells projected to the ipsilateral t.s. at levels rostral to the obex (shortest antidromic latencies 1·4 and 1·8 ms), stimulation was applied in several, closely spaced penetrations close to the mid line, both ipsi- and contralaterally, at levels caudal to the obex. No branches of p.s.r.s were detected in this region.

One p.s.r. was mapped in sufficient detail to allow a reconstruction of its central projection pattern (Fig. 8). The most prominent projection was detected in the ventrolateral n.t.s. Two medial branches were also found at the same dorsoventral level as the t.s. Caudal to 1 mm in front of the obex, we were unable to identify the

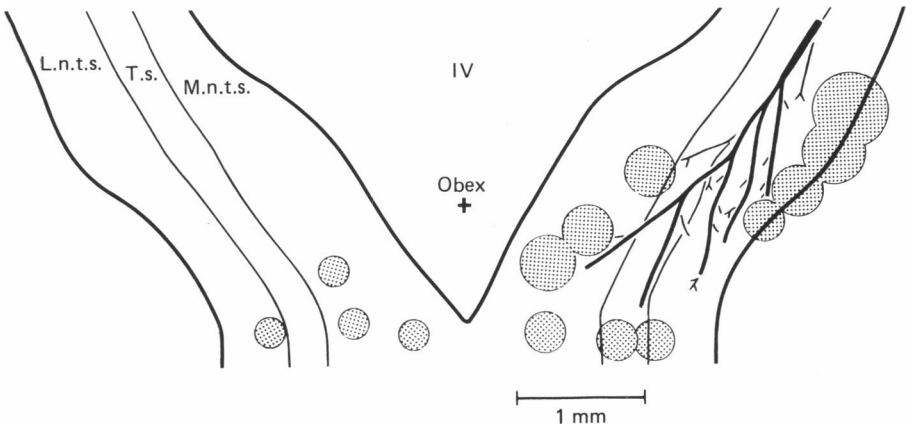


Fig. 8. Projection pattern of a p.s.r. Most branches were found in the ventrolateral n.t.s. Note that the cell has several major branches of similar thickness (as judged from the conduction velocity measurements) coursing within the ventrolateral n.t.s. in parallel to the t.s., rather than one main axon from which thinner collaterals arise. No contralateral projection was found for this cell.

main axon of the cell. Rather, we found four major collaterals which coursed almost in parallel to the t.s. on its lateral side. All had similar conduction velocities (range: 3·4–5·4 m/s). Some thin branches were detected both medially and laterally to the t.s. A few had $A$ coefficients in the range of 2000–4700 $\mu A/mm^2$, thus presumably were located close to the terminals. The thin branches, however, must have been relatively short, as the difference between the longest and the shortest latencies did not exceed 0·9 ms. Alternatively, this limited range of latencies could have resulted from an intermingling of thin and thick branches. With such an arrangement and the difference in the effective current spread for thin and thick fibres stressed throughout this paper, the chance of stimulating a thin branch without first exciting a thicker one (with a shorter latency) is likely to be low.

## DISCUSSION

The primary aim of this study was to map the central projections of r.a.r.s. In all ten r.a.r. cells studied, the densest branching was located on the ipsilateral side in the ventral portion of the medial part of the cadual n.t.s. Typically, at least one primary branch was traced to the contralateral nucleus. In some cells, less dense branching was seen lateral to the t.s.; in only three cells did these branches reach the ventrolateral n.t.s. In addition, this study proved suitable for a more general evaluation of the limitations of the antidromic mapping technique as applied to slowly conducting fibres. The resolution of the method when applied to fibres having a wide range of conduction velocities (fibre diameters) has always been a major methodological concern. Our analysis of current spread and the use of our data to extend previously reported relationships between conduction velocity and the shape of the depth–threshold curves suggest that a single, relatively simple, formula may be used to evaluate conduction velocities (and thus fibre diameters) over a wide range of fibres, once the shape of the depth–threshold curve has been determined.

*Relationship between the effective current spread and conduction velocity*

Most studies in which the current–distance relationships were examined have shown that the threshold–distance curves are of a parabolic rather than a linear shape (Armstrong *et al.* 1973; Shinoda *et al.* 1976; Marcus *et al.* 1979; Hentall *et al.* 1984; see Ranck, 1975 and Lipski, 1981 for reviews). An inverse relationship between $v$ and the slope of the depth–threshold curve had been suggested (BeMent & Ranck, 1969; Jankowska & Roberts, 1972; Roberts & Smith, 1973; Gustafsson & Jankowska, 1976; Shinoda *et al.* 1976). In those studies, the evaluation of the effective current spread was usually made on the basis of either the maximum width of individual depth–threshold curves (most often the widest curves having the lowest thresholds) or by linear interpolation of the experimental data for relatively large distances from the stimulated fibre. In each individual study these methods were appropriate for the particular fibre group examined, but the results could not be applied with certainty to other fibre systems. In the present study application of a second-order equation (cf. Armstrong *et al.* 1973; Merrill, 1974; Shinoda *et al.* 1976; Marcus *et al.* 1979; Hentall *et al.* 1984) allowed us to confirm the parabolic shape of the threshold–distance relationship on a large sample of curves and to use the $A$ coefficient as a measure of the effective current spread for a given fibre regardless of the minimum threshold encountered in each individual penetration. Moreover, if the $A$ coefficient is inversely related to $v$, as it appears to be both from earlier and the present studies, the fibres that we dealt with were more suitable for a quantitative analysis of the $A$–$v$ relationship than those studied earlier. This results from the inverse relationship between $v$ and the $A$ coefficient; the lower the range of $v$, the steeper, and thus easier to notice and measure, the corresponding change of the $A$ coefficient.

The analysis of the combined data from the present study and those reported earlier has led to a simple relationship between $A$ and $v$: $\log A = -1{\cdot}03 \log(v) + 3{\cdot}81$. Use of the relationship allows one to predict the current spread by monopolar microstimulation once the conduction velocity of the stimulated fibre is known, or alternatively, to estimate the conduction velocity once the depth–threshold curve has been determined. Due to the fact that the value of the $A$ coefficient, as determined from individual penetrations, can in extreme cases vary up to 3-fold (see below), the range of 3–35 m/s is the most useful for practical purposes as $A$ changes more than 10-fold within that range. At lower conduction velocities the $A$–$v$ relationship may contain a large error.

It is also noteworthy that the original equation may be transformed into a simpler formula: $A = 6500/v$, where $A$ is expressed in $\mu A/mm^2$. The latter is particularly easy to use and, within the range of 3–35 m/s, should allow one to estimate the effective current spread for different fibres with a deviation of less than 15% from the original equation. In the present study, a fixed latency of response throughout the penetration was regarded as proof that the fibre was activated at a fixed locus. If the criterion of a fixed latency is relaxed, or the fibre conduction velocity is high enough for a shift of the excitation site to be unrecognizable from the latency change, the resulting value of the $A$ coefficient will be underestimated and this in turn will lead to over-estimation of conduction velocity as determined from the $A$–$v$ curve.

The tempting simplicity of the equation, however, must be treated with caution. First, our experience has shown that $A$ coefficients obtained for the same segment of the fibre from several closely spaced penetrations may display a scatter of values of up to 50 % about the mean (see Fig. 3). Differences in tissue impedance or in the excitability of neighbouring nodes of Ranvier may account for these variations (see BeMent & Ranck, 1969; Jankowska & Roberts, 1972 for the discussion of the tissue impedance issue). Secondly, a theoretical consideration of the current spread–conduction velocity relationship (BeMent & Ranck, 1969) suggests that the function may be non-linear, and steeper for low conduction velocities than is proposed in the present paper. However, the non-linear function was based on experimental data obtained by surface stimulation from distances larger than half the internode distance and verified only for conduction velocities between 23 and 85 m/s. Thus, the linear relationship that we found may be an over-simplification and biased by conditions typical for fibres travelling in the white matter since most of the data that we utilized to derive the equation was collected from fibre tracts. On the other hand, the fact that our equation is based entirely on experimental data makes it attractive for practical use because it requires no arbitrary assumptions. It is also noteworthy that a recent study by Hentall *et al.* (1984), involving the direct stimulation of cell bodies (most likely at their axon hillocks), shows a highly significant negative correlation between $A$ and $v$ that quantitatively is similar to ours. The depth–threshold curves obtained by Ahlsén (1984) from fibres having a conduction velocity of less than 0·2 m/s displayed $A$ coefficients that approached 3000 $\mu$A/mm$^2$. Since the course of the stimulating electrode was parallel to that of the fibre, our estimation of the slopes may be too low; nevertheless, the depth–threshold curves for slowly conducting fibres are again seen to be very narrow. There is, however, a clear need for verification of our equation, particularly in the low conduction velocity range. Some slowly conducting pathways in the white matter of the spinal cord would be good candidates for study since the interpretation of the results is simplified by the orderly course of the fibres in the cord, and the white matter of the cord is a more homogenous medium than the medullary area from which our data were collected. One such study, on raphespinal autonomic pathways has just been published (Morrison & Gebber, 1985).

*Distribution of r.a.r. projection*

With regard to mechanical threshold and receptor location, the r.a.r. neurones that we mapped had characteristics typical of the total population we studied. The mean conduction velocity of the cells we studied (about 15 m/s) is lower than the 25 m/s reported by Paintal (see Paintal, 1973, 1984 for reviews). This discrepancy may be explained, at least in part, by the relatively low temperature of the paraffin pool around the vagus nerve in our experiments (about 28 °C). At this temperature, a 30 % drop of conduction velocity in vagal afferent fibres may be expected (Paintal, 1965; see also Paintal, 1973 for the discussion of conduction velocity measurements in other studies). Moreover, since our determinations of conduction velocity were based on the recording of evoked action potentials from the cell body in the ganglion, there is the possibility that the invasion of the soma required some additional time due to a decreased safety factor for impulse transmission at the transition zone between

the medullated fibre and the cell body (see Lipski, 1981). In that case, conduction velocities determined by recording from cell bodies would lead to an underestimation. In a few instances in the course of the present study, by a juxtacellular recording, we observed a deflexion on the rising slope of the evoked spike in cells of the nodose ganglion lasting about 0·1–0·2 ms. Similar, non-linear rising slopes were seen in action potentials recorded intracellularly from petrosal ganglion neurones by Belmonte & Gallego (1983). After corrections, the conduction velocity in peripheral fibres of r.a.r.s in the present study is slightly higher than 21 m/s, close to the value reported by Paintal (1973, 1984). The average conduction velocity for the axons of r.a.r. neurones within the t.s. was 7·8 m/s, and thus about one-third of that in the periphery. A similar conduction velocity drop was described for p.s.r. afferents (Berger & Averill, 1983). It should also be noted that the vagal conduction velocities of p.s.r. fibres reported here must have been similarly underestimated due to the factors discussed above.

The tracheal pressure thresholds at which the mapped receptors began to fire ranged from 5·2 to 34 $cmH_2O$ (average: 15 $cmH_2O \pm 5$ (S.D.)). The corresponding volume of inflation (above end-expiratory) was greater than 37 ml for all but one cell. This is greater than the normal tidal volume of cats. All the cells we mapped had an adaptation index of 90–100 % in response to a fast rising, then maintained lung inflation, and thus were classified as r.a.r.s. The mechanical thresholds and conduction velocities of the cells dealt with in the present study clearly differed from those of low-threshold, slowly adapting p.s.r.s which are the most frequently encountered cells with myelinated axons in the nodose ganglion.

Finally, for six out of seven mapped cells tested by mechanical probing, the receptive field was localized in either the cranial or caudal lung lobes, presumably in intrapulmonary airways. Although the properties of the intra- and extrapulmonary receptors are identical (Mills, Sellick & Widdicombe, 1970), there may be differences in their central projection patterns; this was not examined.

The maximum rostrocaudal extent where we found branches of individual r.a.r. cells was from 1·5 mm cranial to the obex to 2·3 mm caudal. Characteristic features of the central ramification pattern of r.a.r.s were: a main axon travelling within the t.s. rostral to the obex, and a branching point at the level of the obex with at least one major collateral reaching the contralateral nucleus and one descending further ipsilaterally. Within the over-all projection area, the density of branching was not evenly distributed. All but one cell had its densest branching in the ipsilateral nucleus, medial to the t.s., in the region located 0·3–1·3 mm caudal to the obex. Typically, the less developed contralateral projection was restricted to the corresponding area. A less dense projection was found to the medial n.t.s. at levels rostral to the obex. In six afferents, a few collaterals were detected lateral to the t.s. In three of these, signs of branching were found in the ventrolateral n.t.s. rostral to the obex. This is the site of a dense population of inspiratory cells referred to as the dorsal respiratory group. Some of these inspiratory cells have been shown to be excited monosynaptically by p.s.r. afferents (Averill, Cameron & Berger, 1984; Backman, Anders, Ballantyne, Röhrig, Camerer, Mifflin, Jordan, Dickhaus, Spyer & Richter, 1984). The majority send descending axons to the phrenic motor nucleus (Lipski, Kubin & Jodkowski,

1983). Thus, our results suggest the possibility of a direct excitatory action by some r.a.r.s on inspiratory cells of the dorsal respiratory group and, in turn, on phrenic motoneurones. Such a connexion could be responsible for the excitatory, paradoxical response in the phrenic nerve to lung hyperinflation and for the facilitation of the phrenic output during normal hyperpnoeic states (see Paintal, 1973; Pack, 1981; Widdicombe, 1982 for references). However, branching of r.a.r. afferents within the dorsal respiratory group was found in only one-third of the cells and was relatively sparse when compared to the dense projection consistently observed in the commissural n.t.s. The latter region seems to be the main target of r.a.r. afferents. The cells of this subnucleus are small and difficult to record from; so far there are no data on the characteristics, or even the presence, of second-order neurones that subserve the reflexes of r.a.r. origin. Nevertheless, our results suggest that the commissural subnucleus may play an important role in r.a.r. reflexes.

In the present study, we have confirmed that the central projection of p.s.r.s, unlike r.a.r.s, is limited to the ipsilateral n.t.s., as was reported Donoghue *et al.* (1982) and Berger & Averill (1983). These authors showed that the projection of p.s.r.s was mostly to the ventrolateral and medial n.t.s. (also seen in the p.s.r. that we mapped, Fig. 8). Some r.a.r.s have projections to these same regions. However, a comparison of the over-all projection patterns of both receptor types suggests that there is only a limited overlap; r.a.r.s show the densest branching within the commissural subnucleus, a region more caudal to the sites where p.s.r. branches were described. A second feature that distinguishes the central projection patterns is that r.a.r.s project to the contralateral n.t.s. Also, while it is still a matter of controversy whether individual p.s.r.s do (Donoghue *et al.* 1982; this study), or do not (Berger & Averill, 1983) project to more than one subnucleus of the n.t.s., all studies indicate that p.s.r.s display a relatively limited projection. This study indicates that individual r.a.r.s have a widespread projection to different regions of the n.t.s. Finally, comparison of the range of $A$ coefficients found for r.a.r.s and p.s.r.s suggests that fine (possibly terminal) branches of p.s.r.s may be shorter than those of r.a.r.s, or alternatively the latter may have longer non-myelinated terminal portions. These data are of interest in view of the hypothesis advanced by Paintal (1984) that the distinction between p.s.r.s and r.a.r.s may not be a very sharp one. The hypothesis is based, however, on comparisons of the properties of the receptors themselves and their reflex effects as observed at the output of the respiratory system. Our data, which deal with the central projection patterns, suggest that the differences between r.a.r.s and p.s.r.s are quite substantial. To resolve this requires a detailed assessment of the central connexions and relays of both receptor types as well as the extent of their convergence on second-order neurones.

We wish to acknowledge the important contributions of Dr Allan I. Pack; he suggested the study and has provided continuous, helpful discussions. We are grateful to Dr Elzbieta Jankowska for her critical comments on an earlier version of the manuscript, and to Dr Alfred P. Fishman for making the study possible and for encouragement and advice. We thank Mr Daniel C. Barrett for typing the manuscript and Ms Christina Rossiter for technical assistance. L.K. is on leave from the Department of Human Physiology, Warsaw Medical Academy, Poland. This study was supported by a program project grant from the National Heart, Lung and Blood Institute (HL-08805) and from the Division of Research Resources (BRSG SO7 R05464).

REFERENCES

AHLSÉN, G. (1984). Brain stem neurones with differential projection to functional subregions of the dorsal lateral geniculate complex in the cat. *Neuroscience* **12**, 817–838.

ARMSTRONG, D. M., HARVEY, R. J. & SCHILD, R. F. (1973). The spatial organisation of climbing fibre branching in the cat cerebellum. *Experimental Brain Research* **18**, 40–58.

AVERILL, D. B., CAMERON, W. E. & BERGER, A. J. (1984). Monosynaptic excitation of dorsal medullary neurones by slowly adapting pulmonary stretch receptors. *Journal of Neurophysiology* **52**, 771–785.

BACKMAN, S. B., ANDERS, C., BALLANTYNE, D., RÖHRIG, N., CAMERER, H., MIFFLIN, S., JORDAN, D., DICKHAUS, H., SPYER, K. M. & RICHTER, D. W. (1984). Evidence for a monosynaptic connection between slowly adapting pulmonary stretch receptor afferents and inspiratory beta neurones. *Pflügers Archiv* **402**, 129–136.

BELMONTE, C. & GALLEGO, R. (1983). Membrane properties of cat sensory neurones with chemoreceptor and baroreceptor endings. *Journal of Physiology* **342**, 603–614.

BEMENT, S. L. & RANCK JR, J. B. (1969). A model for electrical stimulation of central myelinated fibres with monopolar electrodes. *Experimental Neurology* **24**, 171–186.

BERGER, A. J. & AVERILL, D. B. (1983). Projection of single pulmonary stretch receptors to solitary tract region. *Journal of Neurophysiology* **49**, 819–830.

COTTLE, M. K. (1964). Degeneration studies of primary afferents of IXth and Xth cranial nerves in the cat. *Journal of Comparative Neurology* **122**, 329–345.

DONOGHUE, S., GARCIA, M., JORDAN, D. & SPYER, K. M. (1982). The brain-stem projections of pulmonary afferent neurones in cats and rabbits. *Journal of Physiology* **322**, 353–363.

GREEN, J. D. (1958). A simple microelectrode for recording from the central nervous system. *Nature* **182**, 962.

GUSTAFSSON, B. & JANKOWSKA, E. (1976). Direct and indirect activation of nerve cells by electrical pulses applied extracellularly. *Journal of Physiology* **258**, 33–61.

HENTALL, I. D., ZORMAN, G., KANSKY, S. & FIELDS, H. L. (1984). Relations among threshold, spike height, electrode distance, and conduction velocity in electrical stimulation of certain medullospinal neurones. *Journal of Neurophysiology* **51**, 968–977.

JANKOWSKA, E. & ROBERTS, W. J. (1972). An electrophysiological demonstration of the axonal projections of single spinal interneurones in the cat. *Journal of Physiology* **222**, 597–622.

JANKOWSKA, E. & SMITH, D. O. (1973). Antidromic activation of Renshaw cells and their axonal projections. *Acta physiologica scandinavica* **88**, 198–214.

KALIA, M. & MESULAM, M.-M. (1980). Brain stem projections of sensory and motor components of the vagus complex in the cat. I. The cervical vagus and nodose ganglion. *Journal of Comparative Neurology* **193**, 435–465.

KERR, F. W. L. (1962). Facial, vagal, and glossopharyngeal nerves in the cat. *Archives of Neurology* **6**, 264–281.

KIRSTEN, E. B. & ST. JOHN, W. M. (1978). A feline decerebration technique with low mortality and long-term homeostasis. *Journal of Pharmacological Methods* **1**, 263–268.

KUBIN, L. & DAVIES, R. O. (1984). Distribution and termination of pulmonary rapidly adapting receptor (RAR) neurones in the medulla of the cat. *Federation Proceedings* **43**, 903.

KUBIN, L. & DAVIES, R. O. (1985). Antidromic mapping of the brainstem projection of pulmonary rapidly adapting receptor neurones in the cat. In *Neurogenesis of Central Respiratory Rhythm*, ed. BIANCHI, A. L. & DENAVIT-SAUBIÉ, M., pp. 262–265, Lancaster: Mn.T.P. Press.

LIPSKI, J. (1981). Antidromic activation of neurones as an analytic tool in the study of the central nervous system. *Journal of Neuroscience Methods* **4**, 1–32.

LIPSKI, J., KUBIN, L. & JODKOWSKI, J. (1983). Synaptic action of R-beta neurones on phrenic motoneurones studied with spike-triggered averaging. *Brain Research* **288**, 105–118.

LOEWY, A. D. & BURTON, H. (1978). Nuclei of the solitary tract: efferent projections to the lower brain stem and spinal cord of the cat. *Journal of Comparative Neurology* **181**, 421–450.

MARCUS, S., ZARZECKI, P. & ASANUMA, H. (1979). An estimate of effective spread of stimulating current. *Experimental Brain Research* **34**, 68–72.

MARINO, P. L., DAVIES, R. O. & PACK, A. I. (1981). The responses of $I_\beta$ cells to increases in the rate of lung inflation. *Brain Research* **219**, 289–305.

MERRILL, E. G. (1974). Finding a respiratory function for the medullary respiratory neurones. In *Essays on the Nervous System*, ed. BELLAIRS, R. & GRAY, E. G., pp. 451–486. Oxford: Clarendon Press.

MILLS, J. E., SELLICK, H. & WIDDICOMBE, J. G. (1970). In *Breathing: Hering-Breuer Centenary Symposium*, ed. PORTER, R., pp. 77–92. London: Churchill.

MORRISON, S. F. & GEBBER, G. L. (1985). Axonal branching patterns and funicular trajectories of raphespinal sympathoinhibitory neurones. *Journal of Neurophysiology* **53**, 759–772.

PACK, A. I. (1981). Sensory inputs to the medulla. *Annual Review of Physiology* **43**, 73–90.

PAINTAL, A. S. (1965). Effects of temperature on conduction in single vagal and saphenous myelinated nerve fibres of the cat. *Journal of Physiology* **180**, 20–49.

PAINTAL, A. S. (1973). Vagal sensory receptors and their reflex effects. *Physiological Reviews* **53**, 159–227.

PAINTAL, A. S. (1984). Lung and airway receptors. In *Control of Respiration*, ed. PALLOT, D. J., pp. 78–107. London: Croom Helm.

RANCK JR, J. B. (1975). Which elements are excited in electrical stimulation of mammalian central nervous system: a review. *Brain Research* **98**, 417–440.

ROBERTS, W. J. & SMITH, D. O. (1973). Analysis of threshold currents during microstimulation of fibres in the spinal cord. *Acta physiologica scandinavica* **89**, 384–394.

SANT 'AMBROGIO, G. (1982). Information arising from the tracheobronchial tree of mammals. *Physiological Reviews* **62**, 531–569.

SHINODA, Y., ARNOLD, A. P. & ASANUMA, H. (1976). Spinal branching of corticospinal axons in the cat. *Experimental Brain Research* **26**, 215–234.

WIDDICOMBE, J. G. (1954). Receptors in the trachea and bronchi of the cat. *Journal of Physiology* **123**, 71–104.

WIDDICOMBE, J. G. (1982). Pulmonary and respiratory tract receptors. *Journal of Experimental Biology* **100**, 41–57.